Dynamics and vibration analysis of the interface between a non-rigid sphere and omnidirectional wheel actuators

A. Weiss†*, R. G. Langlois‡ and M. J. D. Hayes‡

†*Department of Mechanical Engineering, Braude Academic College, 51 Snunit St., Karmiel, Israel*
‡*Department of Mechanical and Aerospace Engineering, Carleton University, 1125 Colonel By Drive, Ottawa, ON K1S 5B6, Canada*

SUMMARY

This paper presents analysis of the dynamics and vibration of an orientation motion platform utilizing a sphere actuated by omnidirectional wheels. The purpose of the analysis is to serve as a design tool for the construction of a six-degree-of-freedom motion platform with unlimited rotational motion. The equations of motion are presented taking flexibility of the system into account. The behaviour of the system is illustrated by sample configurations with a range of omnidirectional wheel types and geometries. Vibration analysis follows, and sensitivity to various parameters is investigated. It is determined that the geometry of omnidirectional wheels has a significant effect on the behaviour of the system.

KEYWORDS: Parallel manipulators; Robot dynamics; Motion platform; Rotational motion; Orientation control; Omnidirectional wheels.

1. Introduction

Conventional training simulator motion platforms commonly use a Gough–Stewart platform,[1, 2] otherwise known as a hexapod, to provide motion cues. A hexapod is a mechanical system with six extensible legs arranged in a parallel configuration connecting a moving platform (flying frame) to a fixed base. Positions and orientations of the moving platform are manipulated with six degrees of freedom (6 DOF) by changing the lengths of six prismatic legs. Figure 1 shows a typical example. Various configurations based on this architecture exist. Variation often attempt to expand the workspace of the manipulator and reduce issues related to singularities within the workspace. The reason for the limits and some singularities of the workspace of parallel manipulators lies in the hardware limits of this type of motion platform; however, there are other areas that are suboptimal. These areas have to do mostly with the complicated kinematics of such platforms. The kinematic expressions are mathematically complex, and in many cases, require numerical solutions. In addition, the translational and rotational degrees of freedom are heavily coupled, a fact that further increases the complexity of equations, and consequently increases the computational resources required to evaluate them.

The design of the innovative Atlas motion platform aims to resolve the aforementioned issues, namely, remove singularities from the interior of the reachable workspace, remove the rotational limits, decouple the rotational and translational degrees of freedom, and have a simple kinematic model. Few kinematic architectures addressing some of the aforementioned problems are in development, such as the Eclipse II[3] and the Desdemona.[4] The new platform suggested here is broken down into two different mechanisms sitting one on top of the other: a translational platform and a rotational platform, as shown in Fig. 2. The first is a simple, well-known, XYZ platform that can be implemented in any number of established ways. The latter is a novel design, where a sphere rests on three wheels, and motion is provided with friction at the sphere–wheel interface.

* Corresponding author. E-mail: avi@braude.ac.il

Fig. 1. CAE's version of the Gough–Stewart motion platform for a flight simulator.
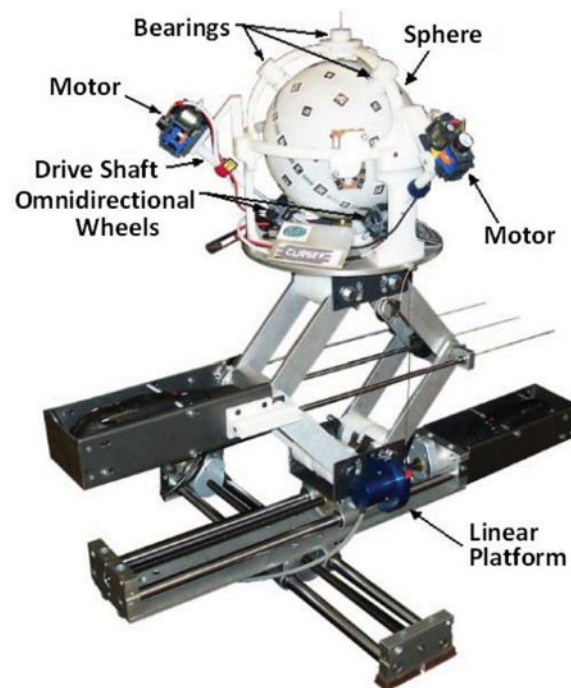

Fig. 2. The Atlas demonstrator.

Different linear combinations of angular speeds of the wheels yield different angular velocity vectors for the sphere. This suggested new platform has the potential, under certain conditions that need to be precisely defined, to open the workspace to become rotationally unlimited while eliminating interior singularities. Other benefits that can be derived from this design are the decoupling of the rotational degrees of freedom from the translational ones, and the compact analytical expressions resulting for the kinematics of the system. This system, however, is not without potential problems. Friction wheels, while offering unlimited range of motion, resist motion in the direction normal to their rotation axis. Instead, omnidirectional wheels with free spinning passive castor rollers on their

periphery, which minimize the resisting friction in the directions normal to their rotation, are used. Various omnidirectional wheel designs exist, each with its respective pros and cons.

Driving a sphere using a combination of magnets and electromagnets was presented in ref. [5], but in a form of a spherical stepper motor which does not allow for continuous smooth motion. Utilizing friction wheels to drive a sphere is also presented by Lauwers *et al.*[6] with simple friction wheels, and by Ferrier and Raucent,[7] where a sphere is actuated for a single degree of freedom by means of a single omnidirectional wheel. The work of West and Asada[8] shows how to use a ball wheel for single degree of freedom actuation with the remaining degrees of freedom passive such that there is no slip. Three such ball wheels may be utilized similarly with omnidirectional wheels with rollers on their periphery to drive a wheeled mobile robot on a plane. Similarly, Williams *et al.*[9] and Saha *et al.*[10] utilize three omnidirectional wheels to drive a mobile robot or vehicle on a plane. Most of the research involving omnidirectional wheels concentrate on wheeled mobile robots, assume perfectly shaped omnidirectional wheels, and discuss the kinematics and dynamics of the platform utilizing 'geometrically perfect' wheels.

The kinematics of the Atlas parallel motion platform, described in ref. [11], was discussed in depth in ref. [12]. In order to utilize the advantageous kinematics of the system, though, attention must be paid to the kinetics of the system. While idealization of the system makes the dynamics appear to be appealing, the inherent flaws of omnidirectional wheels must be overcome so that the Atlas concept can be realized. Thus, attention must be paid to the geometric imperfections of the omnidirectional wheel–sphere interface as well as to the fact that the two bodies involved are not necessarily rigid. The resulting motion involves some level of vibration overlaid on top of the idealized behaviour of the system. An investigation of important parameters and their effect on the resulting vibration follows. These parameters are affected by the contact scheme between the sphere and omnidirectional wheels. For this purpose, a Hertzian contact model[13, 14] is used for representing the omnidirectional wheel–sphere elastic interface.

2. System Model

Obtaining general equations of motion for a platform comprising a sphere actuated by omnidirectional wheels, assuming all components are rigid, is the first step towards understanding the dynamics of the system. However, as mentioned earlier, omnidirectional wheels are not ideal by design; that is, they are never exactly round. Other issues that may arise are the rigidity of their mounts and the contact rigidity. Moreover, various types of omnidirectional wheels exist comprising various materials, and having various geometric shapes. All these need to be taken into consideration when constructing the dynamic model and deriving the equations of motion for the system. The model developed in this work takes into account the effects of the shape of omnidirectional wheels, the stiffness of their mounting, and the deflection of the sphere at the contact point. The overall mechanical system is analysed as a combination of a completely rigid system, with a subsystem of springs and dampers to represent the non-rigid elements, while the shape of the wheel is treated as positional input.

This section presents the model and the corresponding equations of motion for the system. A Matlab program was written to integrate the equations numerically. Sample results will be presented and discussed to show the basic dynamic behaviour of the system for the purpose of verification and validation. The program was developed as a simulation tool that is suitable for allowing more thorough research and analysis of the effects of various design parameters on the system's performance. The analysis of all possible design parameters and their effects on all performance indicators is a vast undertaking; thus, a representative analysis will be presented. The purpose of the analysis is to yield understanding of the different effects of the evaluated parameters on the resulting motion of the system, and not to validate a specific designed and built system, since the motion platform may be used for various applications, and thus, while maintaining the same geometry and architecture, have very different parameters such as weight, centre of mass position, stiffness, *etc*. For example, for a flight simulator application, the physique of the pilot affects the weight and position of the centre of mass of the sphere; a change in the equipment of the airplane simulated may change the weight, centre of mass position, and even the stiffness of the spherical shell between two different runs of the same application. It is for this reason that specific experiments are of little value to the designer of such a system.
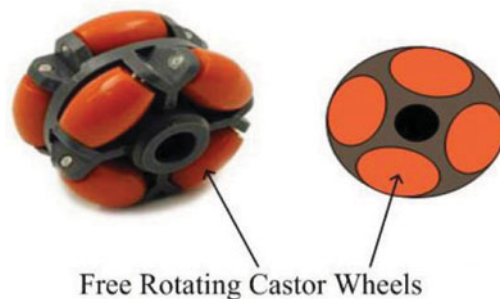
Fig. 3. Dual row omnidirectional wheel.

2.1. Omnidirectional wheel shape

In the suggested platform, omnidirectional wheels act as friction wheels to transmit the motion to the sphere while not resisting motion in the direction orthogonal to the actuation direction. The kinematics of an idealized platform have been derived by the authors for the case where omnidirectional wheels are idealized to a single point of continuous contact with the sphere.[15] In reality, practical omnidirectional wheel design do not support such convenient assumptions. The nature of omnidirectional wheels necessitates discontinuities between the rollers that allow for the extra degree of freedom, leading essentially to the following two alternatives:

1. The first consists of a single row of rollers with some space between the rollers. This results in vibration during actuation due to changes in the local diameter of omnidirectional wheel in gaps where no roller is present. However, the contact point, when present, remains at a single place. This type of wheel is commonly used in mobile robots.[9, 16] Some attempts to solve the vibration issue have been made through either redesigning the omnidirectional wheels to minimize the gaps[17] or going through another level of smooth interface between the omnidirectional wheel and the point of contact by means of a smooth sphere between each actuating omnidirectional wheel and the other surface.[7] An alternative is the Mecanum wheel, where the rollers are at a 45° angle with respect to the main actuation axis of the wheel instead of the more common 90° arrangement.[18, 19]
2. The second alternative consists of two rows of rollers arranged such that a roller is always in contact with the sphere. Designs range from the more commonly available ones, such as shown in Fig. 3, to more sophisticated ones as in ref. [20]. In the dual-row case the point of contact on the sphere varies in time as the contact point switches from one roller to the other and back. This introduces a stepwise oscillation in the instantaneous contact point position vector, thereby altering the kinematics, as presented in detail in ref. [21].

Since kinematic considerations are essential to the core functionality of the motion platform, the omnidirectional wheels modelled in this paper are of the first type, that is, single row omnidirectional wheels. Since one cannot arrange rollers on the periphery of a wheel without having gaps between them, a fairly general description of the wheel and rollers geometry may be seen in Fig. 4. Due to the gap between the rollers, the sphere does not experience smooth motion, but 'falls' into the gaps between rollers. This, in turn, causes the distance between the centre of the sphere and the centre of the omnidirectional wheel to vary as the omnidirectional wheel rotates. In ref. [15], kinematic relationships were developed for the ideal case where omnidirectional wheels were assumed to be perfectly round and there was no relative motion between sphere's and omnidirectional wheels' geometric centres. In addition to the assumption that the omnidirectional wheels and the sphere are rigid, it had also been assumed that the rotational platform is rigidly attached to the translational platform. In order to obtain the equations of motion for a more realistic platform, the kinematics must first be modified to include these departures from the ideal case. First, removing the assumption of a perfectly round omnidirectional wheel means:

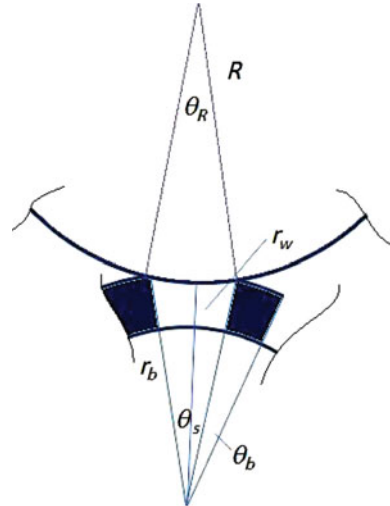$$r_{w_i} = r_{w_i}(\theta_i), \tag{1}$$

Fig. 4. Contact area between omnidirectional wheel and sphere.

thus,

$$\dot{r}_{w_i} = \dot{\theta}_i r'_{w_i}, \tag{2}$$

$$\ddot{r}_{w_i} = \dot{\theta}_i^2 r''_{w_i} + \ddot{\theta}_i r'_{w_i}, \tag{3}$$

where r_{w_i} is the distance from the centre of omnidirectional wheel i to its contact point with the sphere, and θ_i is a cyclical coordinate of the orientation of omnidirectional wheel i, $r'_{w_i} = \frac{\mathrm{d}r_{w_i}}{\mathrm{d}\theta_i}$, and $r''_{w_i} = \frac{\mathrm{d}^2 r_{w_i}}{\mathrm{d}\theta_i^2}$. The actual shape of the omnidirectional wheel has a significant effect on the effective contact radius; however, the radius of the sphere itself also affects the effective contact radius r_{w_i}.

Figure 4 shows the contact area between an omnidirectional wheel and the sphere, illustrating the gaps between the rollers. In this paper, single-race omnidirectional wheels were used to eliminate the step-wise moments injected into the sphere caused by dual-race wheels and instead focus on the effects on the dynamics caused by the geometry of a single race. Here r_b is the maximal radius of the omnidirectional wheel, θ_b is the angular distance between two consecutive rollers, θ_s is the angular size of the gap between two consecutive rollers, both measured about the centre of the omnidirectional wheel, and θ_R is the same gap measured about the centre of the sphere. From geometric considerations, it is apparent that:

$$\sin \frac{\theta_{R_i}}{2} = \frac{r_{b_i}}{R_i} \sin \frac{\theta_{s_i}}{2}. \tag{4}$$

The difference between the maximal and minimal distances between the centres of the sphere and the omnidirectional wheel is

$$\Delta r_{w_i} = (R + r_{b_i}) - \left[\left(R \cos \frac{\theta_{R_i}}{2} \right) + \left(r_{b_i} \cos \frac{\theta_{s_i}}{2} \right) \right]. \tag{5}$$

Thus,

$$\Delta r_{w_i} = R \left(1 - \cos \frac{\theta_{R_i}}{2} \right) + r_{b_i} \left(1 - \cos \frac{\theta_{s_i}}{2} \right), \tag{6}$$

where Δr_{w_i} is defined by the relation

$$r_{w_i} = r_{b_i} - \Delta r_{w_i}. \tag{7}$$

Finally, combining with the constant radius r_{b_i} of the roller area:

$$0 < \theta_i < \theta_{s_i} \quad r_{w_i} = r_{b_i} - \Delta r_{w_i} \sin\left(2\pi \frac{\theta_i}{\theta_{s_i}}\right),$$
$$\theta_{s_i} \leq \theta_i \leq \theta_{s_i} + \theta_{b_i} \quad r_{w_i} = r_{b_i}, \tag{8}$$

where for n_i rollers,

$$\theta_{s_i} + \theta_{b_i} = \frac{2\pi}{n_i}. \tag{9}$$

Defining the roundness ratio η_i as

$$\eta_i = \frac{\theta_{s_i}}{\theta_{s_i} + \theta_{b_i}} \tag{10}$$

provides a means to classify omnidirectional wheels as follows:

- $\eta = 0$ – perfectly round wheel;
- $\eta = 1$ – wheel with continuous contact, such as Mecanum wheels; and
- $0 < \eta < 1$ – omnidirectional wheel with gaps between the rollers where smaller η means smaller gaps.

Thus, Eq. (8) becomes

$$\eta_i = 0; \quad r_{w_i} = r_{b_i},$$
$$\eta_i \neq 0; \quad r_{w_i} = r_{b_i} - \Delta r_{w_i} \sin\left(\frac{n_i \theta_i}{\eta_i}\right). \tag{11}$$

This model essentially presents the main cause for vibration in the system. It should be noted that the effects of omnidirectional wheel's radius changes are small compared with the radius itself (less than 0.5% for typical envisioned implementations), and thus the impact on the Jacobian and the angular motion resulting is negligible. However, its impact on the translational vibratory motion is potentially significant. This model is therefore used in determining the translational motion of the sphere centre.

2.2. Sphere–omnidirectional wheel interface

The interface between omnidirectional wheels and the sphere is treated here as non-rigid. Thus, each contact point is modelled as a combination of a spring and a viscous damper. The non-rigid assumption, in turn, results in each contact point becoming a contact patch that is spread over more than a single point. The implications are that, in addition to radial deflection, there may be two additional resisting moments occurring: rolling resistance and spin resistance. Rolling resistance may be caused due to shifts in the position of the equivalent normal force over a contact patch from the line connecting the centres of the sphere and omnidirectional wheel involved. Spin resistance is due to friction.

2.2.1. Radial deflection.
The radial deflection is modelled as a combination of a spring with linear stiffness K_i and viscous damping C_i. The importance of these coefficients is their contribution to isolation of internal parts of the sphere from vibration. The main source of vibration in the system is the imperfect shape of omnidirectional wheels as they roll in contact with the sphere. Since each contact point is not really connected to others, its effect on the position of the effective centre of the deformed sphere is assumed independent of other contact point deflections. Thus, the radial motion of each contact point is analysed independent of other contact points, and their contributions to the overall translation of the centre of sphere is then vectorially summed to obtain the overall translation of the centre of sphere.

Hertzian Contact Model. Since radial deflection depends on what happens at the contact point, a contact model must be considered. A widely accepted model for this purpose is the Hertzian model.[13,14] The following analysis for the resisting moments is independent of the model of choice, yet an implementation of the Hertzian model is shown as an example. The Hertzian model assumes that the contact patch is circular. In this case, for a normal force N_i at contact point i, the pressure distribution p_i is:

$$p_i = p_{0_i} \sqrt{1 - \left(\frac{r}{a_i}\right)^2}, \tag{12}$$

where r is a local coordinate representing the distance of the point in the contact patch from the centre of contact patch, a is the radius of contact patch and is a function of the equivalent radius R_i' and the equivalent modulus of elasticity E_i'[14] detailed below such that

$$a_i = \left(\frac{3 N_i R_i'}{4 E_i'}\right)^{\frac{1}{3}}, \tag{13}$$

and p_{0_i} is the maximal pressure at the centre of the patch,

$$p_{0_i} = \frac{3 N_i}{2\pi a_i^2}. \tag{14}$$

For this case, the deflection at contact point i is

$$\delta_i = \left(\frac{9 N_i^2}{16 R_i' E_i'^2}\right)^{\frac{1}{3}}. \tag{15}$$

The values of E_i' and R_i' are:

$$E_i' = \frac{E_s E_{w_i}}{E_s(1 - v_{w_i}^2) + E_{w_i}(1 - v_s^2)} \tag{16}$$

and

$$R_i' = \frac{R r_i}{R + r_i}, \tag{17}$$

where E_s and E_{w_i} are Young's moduli of the sphere and omnidirectional wheel i respectively, and v_s and v_{w_i} are the corresponding Poisson ratios.

2.2.2. Rolling resistance. If the equivalent normal force corresponding to the pressure distribution within a contact patch is not located at the corresponding theoretically ideal rigid body contact point, then the normal force would not pass through the geometric centre of the sphere, and therefore create a moment resisting the rolling motion. This, in turn, will affect moment equations, for both sphere and omnidirectional wheels. Various models exist to evaluate the length of the moment arm l_{r_i}. However, it must be included as a contribution to the moment equations of the sphere and omnidirectional wheels:

$$\vec{T}_{r_i} = \vec{l}_{r_i} \times \vec{N}_i \quad i = 1, 2, 3, \tag{18}$$

where $\vec{T}_{r_i}$ is the rolling resistance moment at contact point i and $\vec{l}_{r_i}$ is the position of the equivalent normal force with respect to the rigid body contact point.

Thus, the magnitude of the rolling resistance moment for a single contact point i is:

$$T_{r_i} = -N_i l_{r_i} \quad i = 1, 2, 3 \tag{19}$$

where l_{r_i} is the effective roll moment arm of contact point i, and may be evaluated using either theoretical or experimental models.

The full vector expression of the rolling resistance moment is therefore:

$$\vec{T}_{r_i} = -N_i l_{r_i} \frac{\vec{\Omega} \cdot \hat{\Omega}_i}{|\vec{\Omega} \cdot \hat{\Omega}_i|} \hat{\Omega}_i \quad i = 1, 2, 3. \tag{20}$$

As an illustrative example, the Hertzian model will be used to obtain l_{r_i}. Since the Hertzian model calls for a symmetric distribution of the normal force, the equivalent contact point is at the rigid body contact point; therefore, the normal force passes through the geometric centre of the sphere, and so we obtain:

$$T_{r_i} = 0 \quad i = 1, 2, 3 \tag{21}$$

and clearly,

$$l_{r_i} = 0 \quad i = 1, 2, 3. \tag{22}$$

This result is due to the fact that the Hertzian model is completely symmetrical. This may not necessarily be the realistic case, where possibly $l_{r_i} \neq 0$. However, the moment arm length is limited by the radius of the contact patch. Since l_{r_i} is essentially the centre of pressure offset, it depends on the viscoelastic properties of the interface between the sphere and the omnidirectional wheel, and varies with material properties, speed of rotation, temperature, and other parameters. Practically, this moment arm can be obtained by rolling resistance tests. For demonstration, l_{r_i} will be taken to be $l_{r_i} = a_i$ as long as the angular velocity is non-zero.

2.2.3. Spin resistance. Omnidirectional wheels allow actuation about one axis while providing practically no resistance in a direction perpendicular to the actuation direction. However, they have no mechanism that eliminates resistance in the spin direction. This is due to the assumption that contact occurs at a point. Once the contact point becomes a contact patch, this assumption is no longer valid, and some spin resistance must exist. While specific models for evaluating this component may be considered, it can be modelled as a contribution to the moment equation:

$$T_{s_i} = \iint\limits_{S_i} \mu_i N_i(r, \theta) \, dS_i \quad i = 1, 2, 3, \tag{23}$$

where T_{s_i} is the spin resistance moment at contact point i, and the normal force at the contact point N_i becomes a distributed pressure $N_i(r, \theta)$ over the contact patch S_i, where r and θ are local coordinates at the contact patch surface. The coefficients of dry friction at the contact points are μ_i. As mentioned earlier, various models exist for the evaluation of the distributed normal pressure $N_i(r, \theta)$ and the contact patch shape S_i.

As far as the higher level dynamic model of the platform is concerned, the magnitude of the spin resistance when the angular velocity is non-zero may be modelled as:

$$T_{s_i} = \mu_i N_i l_{s_i} \quad i = 1, 2, 3, \tag{24}$$

where l_{s_i} is the effective spin lever of contact point i, and also may be evaluated using either theoretical or experimental models.

The full vector expression of the spin resistance would therefore be:

$$\vec{T}_{s_i} = \mu_i N_i l_{s_i} \frac{\vec{\Omega} \cdot \vec{R}_i}{|\vec{\Omega} \cdot \vec{R}_i|} \hat{R}_i \quad i = 1, 2, 3. \tag{25}$$

Note that due to this definition of the resisting components

$$\vec{T}_{s_i} \cdot \vec{T}_{r_i} = 0 \quad i = 1, 2, 3. \tag{26}$$

Once more, the Hertzian model will be used to obtain l_{s_i}. Spin is the rotation about the axis that connects the geometric centres of the sphere and an omnidirectional wheel through the contact point. When the contact point becomes a contact patch, spin is accompanied by friction, which is proportional to the normal force at the point. Although the resultant friction force may be zero, the friction produces a moment resisting the spin motion:

$$T_{s_i} = \iint_{c.p.} \mu_i p_i r \, \mathrm{d}S = \int_0^{2\pi} \int_0^{a_i} \mu_i p_i r^2 \mathrm{d}r \mathrm{d}\theta. \tag{27}$$

Using Eq. (12) and applying the integral limits, results in:

$$T_{s_i} = \frac{3\pi}{16} \mu_i N_i \left(\frac{3 N_i R_i'}{4 E_i'} \right)^{\frac{1}{3}}. \tag{28}$$

The direction of the spin resistance is opposite to that of the spin direction at the contact point, thus

$$\vec{T}_{s_i} = -\frac{3\pi}{16} \mu_i N_i \left(\frac{3 N_i R_i'}{4 E_i'} \right)^{\frac{1}{3}} \frac{\vec{\Omega} \cdot \vec{R}_i}{|\vec{\Omega} \cdot \vec{R}_i|} \hat{R}_i, \tag{29}$$

therefore

$$l_{s_i} = \frac{3\pi}{16} \left(\frac{3 N_i R_i'}{4 E_i'} \right)^{\frac{1}{3}} \quad i = 1, 2, 3. \tag{30}$$

The total spin resistance is therefore:

$$\vec{T}_s = \sum_{i=1}^{3} \vec{T}_{s_i}. \tag{31}$$

2.3. Omnidirectional wheel–translational platform interface

Another important interface is the one between the translational platform and omnidirectional wheels. The reaction forces between omnidirectional wheels and the sphere affect the mounting point of the omnidirectional wheel onto the translational platform. The mounting point, which is attached to the omnidirectional wheel's centre, is modelled as non-rigid. Each mounting point is modelled as having stiffness coefficient k_i, and viscous damping coefficient c_i.

Combining the effects of the shape of omnidirectional wheels, the sphere–omnidirectional wheel contact interface, and the omnidirectional wheel–translational platform interface, with the rigid body dynamics makes up the model of the system that allows investigation of the dynamics of the system as well as vibration issues.
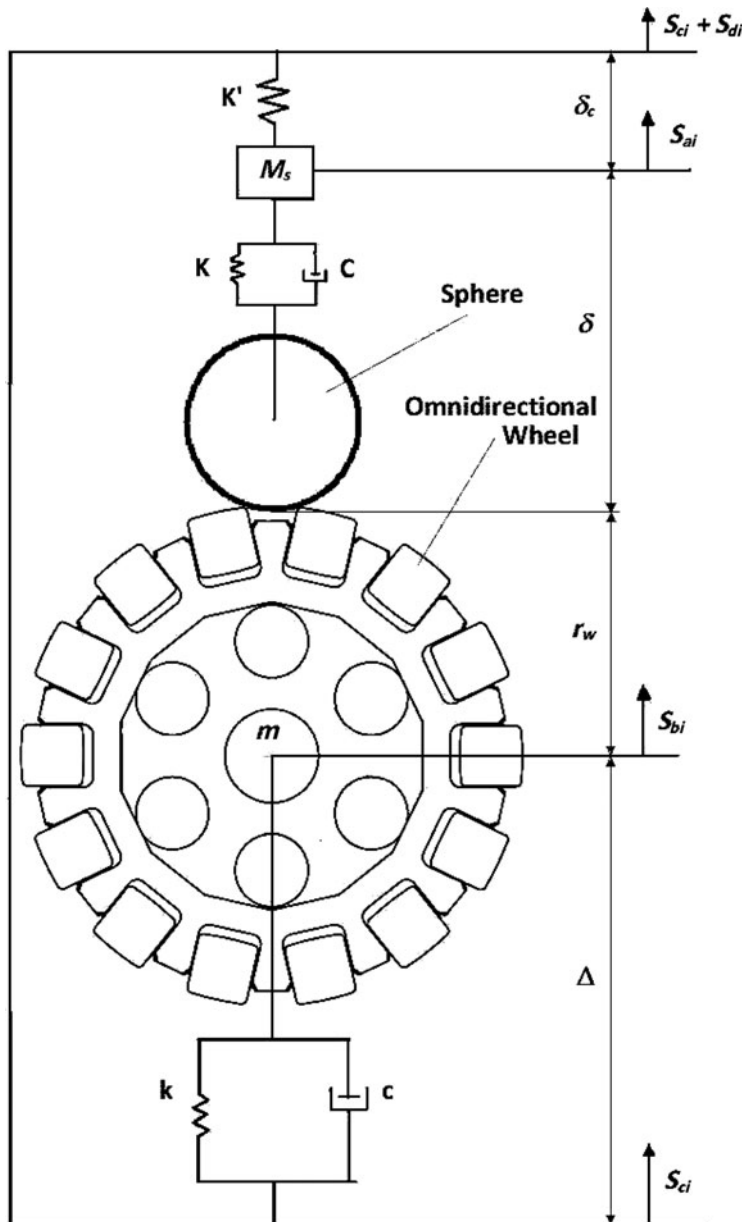
Fig. 5. Model for contact point.

The model for the contact point area is illustrated in Fig. 5. This figure depicts the sphere (disproportionally small) in contact with an omnidirectional wheel (magnified to enhance details at the contact area). The sphere's contact with the omnidirectional wheel is represented as a mass M_s on a spring and damper in parallel, thus the entire sphere is represented by the massless spherical shape marked as 'sphere', the spring–damper combination to model the elastic features of the sphere, and the mass M_s. On top of the sphere there is a spring that ensures contact at all times. The omnidirectional wheel is assumed to be attached to the translational platform through a similar mechanism of spring and damper in parallel. It takes the translational platform's motion (S_{c_i} in the illustration) as a motion input into the sphere. The motion input into the sphere is a combination of the translational motion of the centre of the omnidirectional wheel and the distance to the effective contact point between the sphere and the omnidirectional wheel. All contact points are treated using the same model. Next, the parameters S_{a_i}, S_{b_i}, S_{c_i} need to be mapped into the parameters in the context of the Atlas

platform,

$$S_{a_i} = \vec{R}_s \cdot \hat{r}_{w_i},$$
$$S_{b_i} = \vec{R}_l \cdot \hat{r}_{w_i} + \Delta_i,$$
$$S_{c_i} = \vec{R}_l \cdot \hat{r}_{w_i},$$
$$S_{d_i} = \text{constant}, \tag{32}$$

where $\vec{R}_s$ is the position of the centre of the sphere, $\vec{R}_l$ is the position of the translational platform, Δ_i is the local deflection of the attachment point of the omnidirectional wheel to the translational platform, and S_{d_i} is a constant distance definition of the kinematic closure of the system, $S_{d_i} > 2R$. The exact magnitude is determined by the geometric details and design of the system, and does not impact the results. To obtain vibration information, we observe

$$\Delta\vec{R} = \vec{R}_s - \vec{R}_l, \tag{33}$$

where $\Delta\vec{R}$ is the displacement of the effective centre of the sphere from the geometric centre of a perfect sphere. One can observe that

$$\vec{R}_l \cdot \hat{r}_{w_i} + \Delta_i + r_{w_i} + \delta_i = \vec{R}_s \cdot \hat{r}_{w_i} \tag{34}$$

and kinematic closure equations maintain:

$$\Delta_i + r_{w_i} + \delta_i + \delta_{c_i} = Z_c, \quad \text{and} \tag{35}$$
$$\dot{\Delta}_i + \dot{r}_{w_i} + \dot{\delta}_i + \dot{\delta}_{c_i} = 0. \tag{36}$$

3. Equations of Motion

Utilizing the assumptions and relations described in the previous sections, combined with the kinematic relations, Eqs. (37)–(44) below are obtained using the Newton–Euler dynamic formulation. In order to maintain the model as general and application-independent as much as possible, application-dependent details are generalized. Specifically, the translational motion implementation is treated as a black box controlled by three independent forces along its main axes. In addition, form closure is assumed without detail, and the internal structure of the sphere is also generalized into an arbitrary inertia tensor.

Equations of motion were derived using the Newtonian approach. The system is broken down into two subsystems: the sphere and the translational platform (which includes everything except the sphere).

First, the force equation for the sphere is:

$$\vec{F}_{\text{ext}} + \sum_{i=1}^{3} \vec{N}_i + \sum_{i=1}^{3} \vec{f}_i = M_s(\ddot{\vec{R}}_s), \tag{37}$$

where M_s is the mass of the sphere, $\vec{F}_{\text{ext}}$ is an external compressive force applied to the sphere to ensure zero slip, and $\vec{N}_i$ and $\vec{f}_i$ are the normal and frictional forces at contact point i respectively.

The force equation for the translational platform is:

$$\vec{P} - \sum_{i=1}^{3} \vec{N}_i - \sum_{i=1}^{3} \vec{f}_i = \left(M_l + \sum_{i=1}^{3} m_i\right) \ddot{\vec{R}}_l, \tag{38}$$

where M_l is the mass of the translational platform, m_i is the mass of omnidirectional wheel i, $\vec{P}$ is the force applied to the translational platform, and R_l is the position vector of the mass centre of translational platform. The moment equation of each omnidirectional wheel i about its geometric centre is:

$$T_i - f_i r_{w_i} - T_{r_i} = I_{w_i} \dot{\omega}_i, \tag{39}$$

where T_i is the actuation moment of omnidirectional wheel i. This equation is a scalar equation, and is valid for each of the omnidirectional wheels in the system. In the case where there are three omnidirectional wheels, there are three equations involved. The moment equation of the sphere about its geometric centre is:

$$\sum_{i=1}^{3} \vec{f}_i \times \vec{R}_i - \sum_{i=1}^{3} \vec{T}_{r_i} - \sum_{i=1}^{3} \vec{T}_{s_i} = [I_s] \vec{\dot{\Omega}} + \vec{\Omega} \times [I_s] \vec{\Omega}. \tag{40}$$

Equations for elastic effects at contact points, derived using the model presented in Fig. 5, are:

$$M_s(\vec{\ddot{R}}_l \cdot \hat{r}_{w_i} + \ddot{\Delta}_i + \ddot{\delta}_i) + C_i \dot{\delta}_i + K_i \delta_i - K'_i(\Delta_i + \delta_i) = K'_i(r_{w_i} - Z_c) - M_s \ddot{r}_{w_i}, \tag{41}$$

and

$$m_i \ddot{\Delta}_i - C_i \dot{\delta}_i + c_i \dot{\Delta}_i - K_i \delta_i + k_i \Delta_i = 0. \tag{42}$$

Finally, from the kinematics,

$$\vec{\dot{\Omega}} = J \{\dot{\omega}\}, \tag{43}$$

and the quaternionic differential equation,

$$\dot{q} = \frac{1}{2} \Omega \circ q. \tag{44}$$

It is essential to understand that deviation of the centre of mass from the geometric centre will not result in the coupling of translational and rotational motions due to the fact that the motion of omnidirectional wheels is controlled, and setting the moment applied to them is the only means to cause rotational motion in the system. Thus, as long as the friction limit at contact points is not exceeded, the only effect would be that of increasing reaction forces at contact points. Since it is desired to obtain a slip-free system, the required external force $\vec{F}_{\text{ext}}$ that would yield zero kinetic slip needs to be determined. This is achieved by assuming that the friction limit is exactly reached while still maintaining the kinematic no-slip condition, that is, $f_i = \mu_i N_i$ and $\vec{\dot{\Omega}} = J \{\dot{\omega}\}$. The result is the minimum required external force to assure no-slip condition. In this case,

$$\vec{F}_{\text{ext}} = \frac{M_s}{M_T - M_s} \left(\frac{M_s}{M_T} \vec{P} - R^2 \left([v] - [\mu]^{-1} [R_i]\right) \left([I_w] [r_w]^{-1} [I_s]^{-1} [\Omega]^T [\Omega] + [r_w]\right)^{-1} \{T\} \right), \tag{45}$$

and

$$\{N\} = \left([I_w] R^2 [r_w]^{-1} [I_s]^{-1} [\Omega]^T [\Omega] [\mu] + [r_w] [\mu]\right)^{-1} \{T\}, \tag{46}$$

where $[I_w]$ is a diagonal matrix containing the moments of inertia of omnidirectional wheels, $[I_s]$ is the inertia tensor of the sphere, and $[\mu]$ is the diagonal matrix with μ_i as its elements. In addition, $[R_i]$ is a matrix with $\hat{R}_i$ as its columns, $[v]$ is a matrix with $\hat{v}_i$ as its columns, and $[r_w]$ is a matrix with r_{w_i} as its columns. This set of equations is a combination of differential and algebraic equations. Thus,
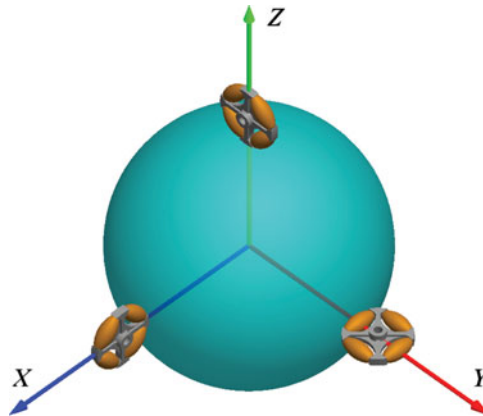
Fig. 6. The orthogonal architecture case.

the differential equations need to be integrated while the algebraic equations need to be solved at each integration step simultaneously. Integration was performed utilizing the basic 4th order Runge–Kutta method (Ode45 solver) in a Matlab program.

Several steps were performed during each integration iteration. First, the orientation of each omnidirectional wheel is translated into the input function for the vibration equations utilizing Eq. (11). Then the actual current omnidirectional wheel radii (r_{w_i}) and their time derivatives are evaluated. Next, the contact forces N_i are evaluated algebraically. Finally, the differential equations are evaluated and the required external force is calculated. At the end of the integration step, constraints are checked and enforced.

3.1. *Verification and validation*

A Matlab program was developed to simulate the dynamics. To verify the program and equations, the orthogonal case presented in ref. [15] was considered. The orthogonal case is presented in Fig. 6, where omnidirectional wheels control mutually orthogonal axes. The goal of this exercise was to qualitatively validate the program by introducing scenarios with predictable results before delving into the analyses of more realistic and complex behaviours.

First, a scenario where all bodies are rigid and omnidirectional wheels are perfectly round is examined as a baseline. Here the expectation is to obtain a pure ideal motion of a sphere rolling without sliding on actuating omnidirectional wheels. The translation should show parabolic motion as a result of a constant driving force. The rotational motion is expected to behave similarly as driven by constant torques, which is to be indicated in Euler parameters behaving in a sinusoidal manner. The resulting angular velocity vector of the sphere is expected to develop linearly. Zero vibration or perturbatory motion is expected is such an ideal system. Observing the above-mentioned resulting motion should verify the basic equations of the motion portion of the model.

Second, to ensure that non-ideal omnidirectional wheel shapes are correctly introduced into the simulation, a basic set of examples with varying values of roundness ratio is offered. The expectation is to observe vibrational motion superimposed on ideal motion. The frequencies are expected to reflect the number of rollers and angular velocity of each omnidirectional wheel. The orthogonal configuration was used so that the three axes would be independent of one another, thus each axis should represent the effects of a single omnidirectional wheel.

Finally, to show the effects of a non-rigid sphere, an effective spring coefficient was considered along with imperfect omnidirectional wheels to show the vibration isolation effects of the model. The expectation is to observe reduction in the maximal magnitude that was observed when a similar omnidirectional wheel was used combined with a rigid sphere.

The baseline configuration is a sphere with radius $R = 1.22$ m, and mass $M_s = 5$ kg. Since in a vibrating system the larger the mass, the less it is affected by external irregularities, low mass was selected for the sphere to enhance any vibrational motion for easier analysis. The translational platform's mass is $M_l = 5$ kg. The three identical wheels have a mass of $m_1 = m_2 = m_3 = 0.25$ kg
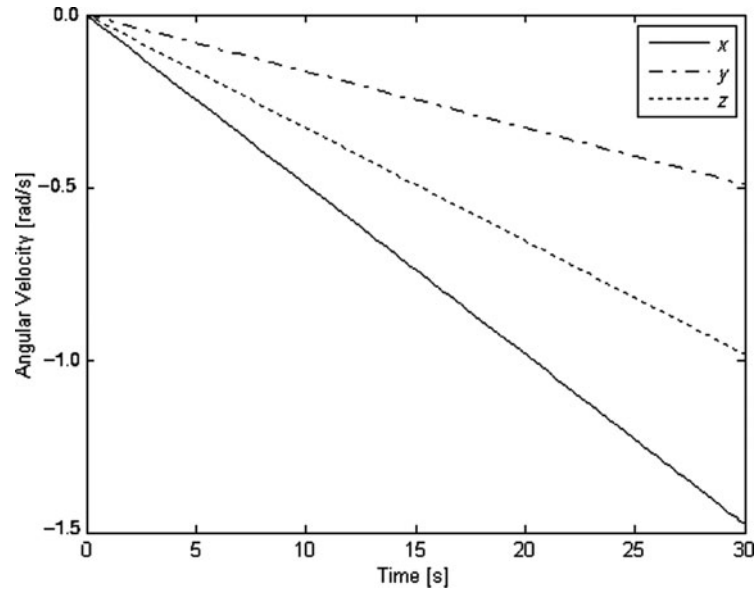
Fig. 7. $\vec{\Omega}$ as a function of time for the orthogonal case.

and nominal radii of $r_{w_1} = r_{w_2} = r_{w_3} = 7.58$ cm. The coefficient of friction at the contact points was taken as a representative value with $\mu = 0.9$.

3.1.1. Ideal case. The most basic results presented are for the ideal case, where all bodies are rigid and the omnidirectional wheels are perfectly round ($\eta = 0$). This case is used for the basic verification of the simulation. The details of the driving forces used for the validation were taken to be step functions, where the magnitudes of the steps are $P_x = 0.1$ N, $P_y = 0.2$ N, $P_z = 0.3$ N, $T_1 = 0.1$ N $\cdot$ m, $T_2 = 0.2$ N $\cdot$ m, and $T_3 = 0.3$ N $\cdot$ m. Figure 7 shows the development of the angular velocity vector components of the sphere. Both translational behaviour and magnitudes behave as predicted since there is no resisting moment acting on the sphere, and the actuating moment is constant.

The components of the quaternion representing the orientation of the sphere are shown in Fig. 8. The harmonic plots represent motion about a constant axis and the increasing frequency indicates an increasing angular velocity as one would expect. The translational portion of the motion, indicated by the position of the centre of mass of translational platform, is presented in Fig. 9. It is expected to develop in a parabolic fashion as there are no resisting forces to oppose the constant applied force $\vec{P}$. It is also clear that there is no indication of coupling between the angular degrees of freedom and the translational ones.

All other components remain at zero level as expected. That is, there is no relative translational motion between the sphere and the translational platform.

3.1.2. Imperfect omnidirectional wheels. In the imperfect omnidirectional wheel case, the omnidirectional wheels are no longer assumed to be perfectly round; however, all system components remain rigid. The goal here is to observe whether the rigid system reacts to the shape input of wheels within the rigid constraints. It is expected that observable relative motion will occur between the centre of the sphere and the translational platform which is of the same magnitude as the input signal, that is, the shape irregularities of omnidirectional wheels. Results show vibration caused by the gaps between the rollers.

The omnidirectional wheels currently in use in the Atlas demonstrator have 14 rollers, and a roundness ratio, $\eta = 0.4485$. The motion of the centre of sphere relative to the translational platform, in the inertial x, y, and z-directions, along with the magnitude of the vector, was simulated. Figure 10, using the real parameters of the Atlas demonstrator, is presented in a dual format, on the left are the raw results, and on the right is the magnification of the graph showing the first 1.5 s of the results revealing more details. Similar plots were obtained for various values of roundness ratio, and it was observed that the lower the roundness ratio, the smoother the motion, since the magnitude of the vibration of the sphere's centre of mass grows larger as the roundness ratio increases. A summary of
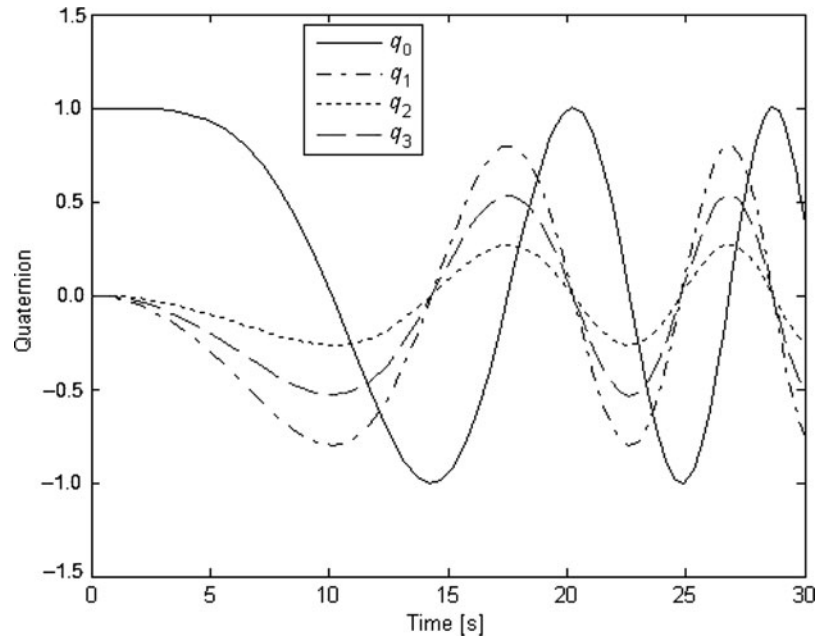
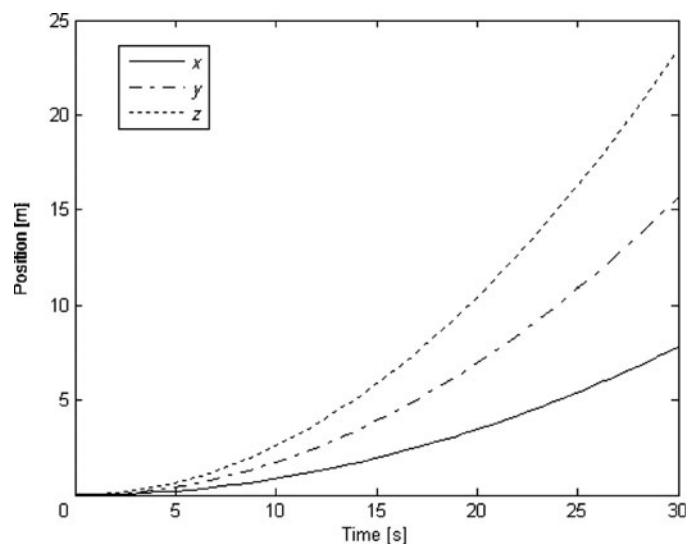Fig. 8. The quaternion as a function of time for the orthogonal case.

Fig. 9. $\vec{R}_l$ as a function of time for the orthogonal case.

these results is illustrated directly in Figs. 10 and 11. Figure 10 also reveals that there is no change in the frequency of the peaks observed in the plots. These results are expected as suggested by Eqs. (6) and (8), where reducing θ_{s_i} and θ_{R_i} reduces Δr_{w_i}, thereby reducing the magnitude of the input perturbation function.

3.1.3. Non-rigid sphere. When considering a non-rigid sphere, the stiffness of the contact point is considered. In this example, the stiffness coefficient was selected to be $K_i = 188,208$ N/m, which is the measured stiffness of the Atlas demonstrator sphere. Figure 12 shows the response for constant angular speed values of $\omega_1 = 0.1$ rad/s, $\omega_2 = 1.2$ rad/s, and $\omega_3 = 0.3$ rad/s for the case where the roundness ratio is $\eta = 0.4485$, but with the above stiffness coefficient. Comparing Fig. 12 with the results illustrated in Figs. 10 and 11 it is to be seen that the magnitude of vibration for the non-rigid sphere is several orders of magnitude lower than that of the rigid system.
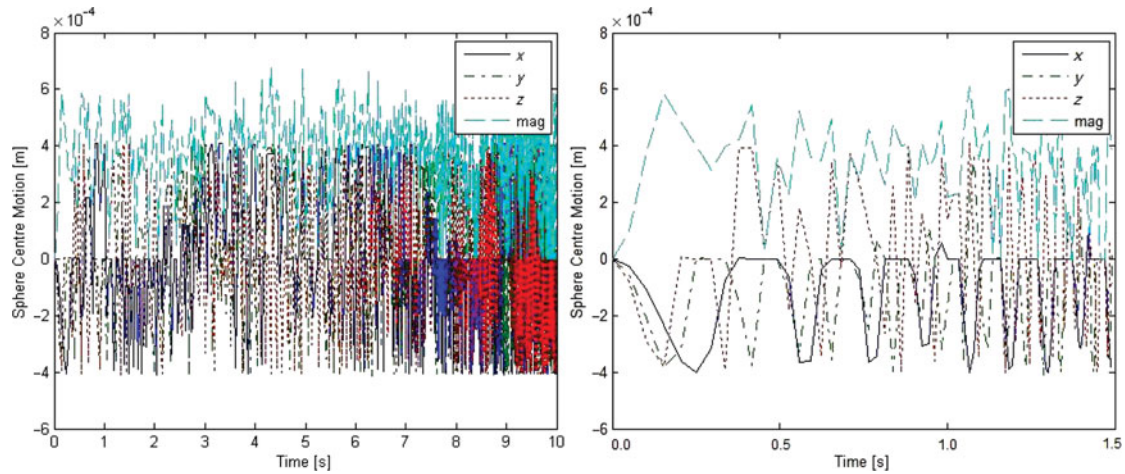
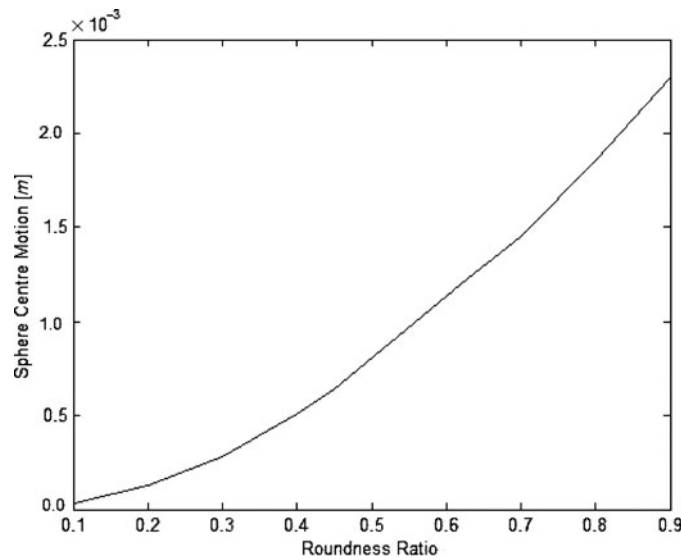Fig. 10. $\Delta \vec{R}$ as a function of time for the orthogonal case, $\eta = 0.4485$.

Fig. 11. Maximum magnitude of $\Delta \vec{R}$ as a function of η for the orthogonal case.

Figure 13 presents the result for the same system but with a damping coefficient of $C_i = 8500 \text{ N} \cdot \text{s/m}$, and Fig. 14 shows results for a damping coefficient of $C_i = 20,000 \text{ N} \cdot \text{s/m}$. Thus, adding damping to the system causes a noticeable but very slight reduction in the magnitude of the vibration. It is observed, though, that adding damping to the system removes the secondary vibration overlaid on top of the main vibration, that is, the high-frequency but lower-magnitude vibration that is observed in Fig. 12 disappears in the plots where damping was introduced. Thus, the importance of the stiffness of sphere is highlighted and is worth further examination, but damping effects seem to be relatively minor.

4. Discussion

The purpose of presenting the simulation results was verification and validation of the simulation program prior to investigate more complex cases. The expected results were stated for the ideal case and the simulation results obtained indeed were as expected. The introduction of non-ideal shape for omnidirectional wheels added vibrations to the system, and it was shown, as expected, that increasing the roundness ratio increases the magnitude of the vibratory motion of the centre of sphere. Removing the rigid body assumption from the sphere introduced vibration isolation effects; and a significant
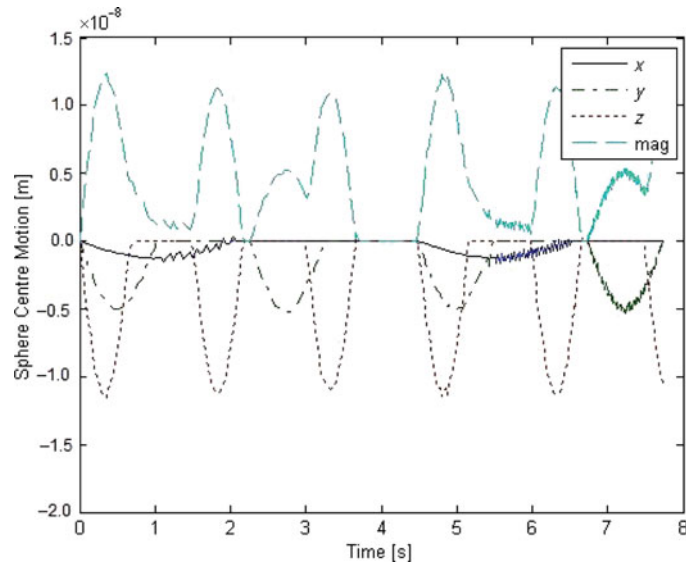
Fig. 12. $\Delta \vec{R}$ as a function of time for the orthogonal case, $\eta = 0.4485$, $K_i = 188208$ N/m.
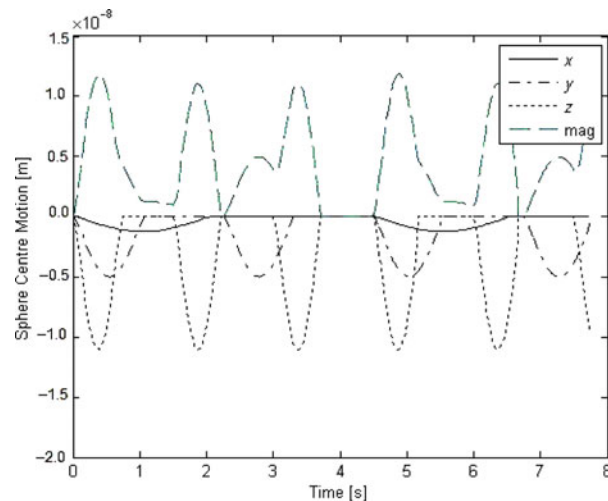

Fig. 13. $\Delta \vec{R}$ as a function of time for the orthogonal case $\eta = 0.4485$, $K_i = 188, 208$ N/m, and $C_i = 8500$ N $\cdot$ s/m.

reduction in the magnitude and frequency of the sphere was observed. Adding damping to the system indeed smoothed the plots more without much affecting the magnitude and frequency of the vibration. All these results were predicted prior to running the simulation program and presented earlier, thus verifying and validating the program for use in more complex scenarios.

It is quite clear from the results that the roundness ratio and the stiffness of the sphere significantly affect the motion of the sphere, as expected and presented in Figs. 11 and 12, while the equivalent damping coefficient at contact point has a less significant role in the resulting motion of the centre of sphere.

5. Conclusions

The kinetics of a sphere actuated using omnidirectional wheels has been explored in a general way for the first time. The number of actuating wheels as well as their type has been considered, and some specific configurations have been explored. Once the kinematics of a system is in place, deriving the equations of motion, assuming that all bodies are rigid, is a relatively straightforward process.
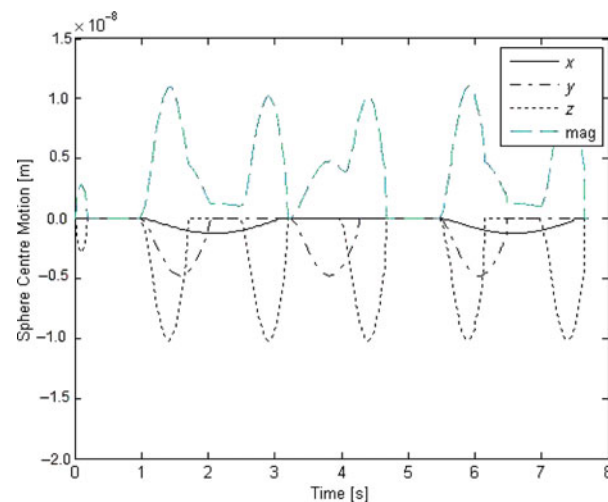
Fig. 14. $\Delta \vec{R}$ as a function of time for the orthogonal case $\eta = 0.4485$, $K_i = 188, 208$ N/m, and $C_i = 20,000$ N · s/m.

However, no system is completely rigid. Specifically with the Atlas platform, it was observed that the sphere–roller interface experiences significant deflections (associated with the low mass design objective and the soft castor rollers material). Thus, it was assumed that the interfaces between the sphere and omnidirectional wheels are non-rigid. In addition, other connection points were assumed flexible. Most interesting is the non-rigid interface at force transfer points; that is, the contact points between the sphere and the actuating omnidirectional wheels. The deflection at the sphere–roller interface causes the contact points to become contact patches with distributed normal and tangential forces. These, in turn, create moments resisting the driving moments in the form of spin resistance and rolling resistance. These moments were modelled as a product of a moment arm and a force. This idea for modelling allowed for the investigation of the effects of the moment arm length on the resisting moments regardless of the model selected to evaluate them. A detailed analysis using the classic Hertzian model for contact forces was performed to demonstrate this approach. However, due to the Hertzian basic assumption that the contact patch is symmetric, rolling resistance vanished. This demonstrated the power of the modelling approach of a moment arm that can be varied to investigate its effect. The results showed only negligible effects of both spin resistance and especially rolling resistance. The effects of elastic contact on the vibration of the centre of sphere were, though, dominant when compared with a rigid sphere, but varied little with changes in the effective spring coefficient of contact. Modelling for vibration assumed that the contact points between the sphere and omnidirectional wheels act like spring–damper systems that are independent of one another, since the actual centre of sphere is not necessarily connected to contact points. The shape of omnidirectional wheels was taken as positional excitation. Similarly, the mounting of omnidirectional wheels onto the linear platform and the contact between the sphere and kinematic closure mounting points were taken as non-rigid. The most significant effect on vibration by far was that of the stiffness of the sphere–wheel contact. It was evident that the effective spring coefficient of this interface is the dominant factor when it comes to natural frequency and maximum vibration magnitude of the centre of sphere's position. The omnidirectional wheel's mounting stiffness had a minor impact on the natural frequency of the system, but not much on the maximal magnitude. The damping coefficient's contribution was also minor.

References
1. V. E. Gough, "Discussion in London: Automobile Stability, Control and Tyre Performance," *Proceedings of the Automotive Division of the Institution of Mechanical Engineers* (1956) pp. 392–394.

2. D. Stewart, "A Platform with 6 Degrees of Freedom," *Proc. Inst. Mech. Eng.* **180**(15, Pt. 1), 371–386 (1965).
3. J. Kim, J. C. Hwang, J. S. Jim, C. C. Iurascu, F. C. Park and Y. M. Cho, "Eclipse II: A new parallel mechanism enabling continuous 360-degree spinning plus three-axis translational motions," *IEEE Trans. Robot. Autom.* **18**(3), 367–373 (Jun. 2002).
4. W. Bles and E. Groen, "The DESDEMONA motion facility: Applications for space research," *Microgravity Sci. Technol.* **21**(4), 281–286 (Nov. 2009).
5. G. S. Chirikjian and D. Stein, "Kinematic design and commutation of a spherical stepper motor," *IEEE/ASME Trans. Mechatronics* **4**(4), 342–353 (Dec. 1999).
6. T. B. Lauwers, G. A. Kantor and R. L. Hollis, "One is Enough!," *Proceedings of 2005 International Symposium of Robotics Research*, San Francisco, CA, USA (Oct. 12–15, 2005).
7. L. Ferriere and B. Raucent, "ROLLMOBS, a New Universal Wheel Concept," *Proceedings of the 1998 IEEE International Conference on Robotics and Automation*, Leuven, Belgium (May 16–20, 1998) pp. 1877–1882.
8. M. West and H. Asada, "Design and Control of Ball Wheel Omnidirectional Vehicles," *Proceedings of the IEEE International Conference on Robotics and Automation*, Nagoya, Japan (May 21–27, 1995) pp. 1931–1938.
9. R. Williams, D. Carter, P. Gallina and G. Rosati, "Dynamics model with slip for wheeled omni-directional robots," *IEEE Trans. Robot. Autom.* **18**(3), 285–293 (2002).
10. K. Saha, J. Angeles and J. Darcovich, "The design of kinematically isotropic rolling robots with omnidirectional wheels," *Mech. Mach. Theory* **30**(8), 1127–1137 (1995).
11. M. J. D. Hayes and R. G. Langlois, "A novel kinematic architecture for six DOF motion platforms," *Trans. Can. Soc. Mech. Eng.* **29**(4), 701–709 (May 2005).
12. A. Weiss, R. G. Langlois and M. J. D. Hayes, "Unified treatment of the kinematic interface between a sphere and omnidirectional wheel actuators," *ASME J. Mech. Robot.* **3**(4), 041001 (Sep. 26, 2011).
13. H. Hertz, "On the contact of elastic solids," *J. Reine und Angewandte Mathematik* **92**, 156–171 (1882).
14. K. L. Johnson, *Contact Mechanics* (Cambridge University Press, New York, NY, 1985).
15. M. J. D. Hayes, R. G. Langlois and A. Weiss, "Atlas motion platform generalized kinematic model," *Meccanica* **46**(1), 17–25 (Jan. 2011).
16. Y. P. Leow, K. H. Low and W. K Loh, "Kinematic Modelling and Analysis of Mobile Robots with Omni-Directional Wheels," *Proceedings of the 7th International Conference on Control, Automation, Robotics and Vision (ICARCV 2002)*, Singapore (Dec. 2–5, 2002) pp. 820–825.
17. J. B. Song and K. S. Byun, "Design and control of a four-wheeled omnidirectional mobile robot with steerable omnidirectional wheels," *J. Robot. Syst.* **21**(4), 193–208 (Apr. 2004).
18. S. L. Dickerson and B. D. Lapin, "Control of an Omni-Directional Robotic Vehicle with Mecanum Wheels," *Proceedings of the 1991 IEEE International Conference on Robotics and Automation*, Atlanta, GA, USA (Mar. 26–27, 1991) pp. 323–328.
19. J. Agullo, S. Cardona and J. Vivancos, "Dynamics of vehicle with directionally sliding wheels," *Mech. Mach. Theory* **24**(1), 53–60 (1989).
20. M. Shugen, R. Chao and Y. Changlong, "An Omnidirectional Mobile Robot: Concept and Analysis," *Proceedings of the 2012 IEEE International Conference on Robotics and Biomimetics (ROBIO)* (2012) pp. 920–925.
21. A. Weiss, R. G. Langlois and M. J. D. Hayes, "The effects of dual-row omnidirectional wheels on the kinematics of the atlas spherical motion platform," *J. Mech. Mach. Theory* **44**(2), 349–358 (Feb. 2009).